Conformational studies of the two anomeric methyl glycosides of α-D-Man*p*-(1→2)-D-Glc*p* by molecular simulations and NMR ^{1}H,^{1}H T-ROESY experiments

Kristina Lycknert, Christer Höög and Göran Widmalm *

Department of Organic Chemistry, Arrhenius Laboratory, Stockholm University, S-106 91 Stockholm, Sweden. E-mail: gw@organ.su.se

Received (in Cambridge, UK) 12th December 2001, Accepted 21st January 2002
First published as an Advance Article on the web 11th February 2002

A conformational study has been performed of the two disaccharides α-D-Man*p*-(1⟶2)-α-D-Glc*p*-OMe (**1**) and α-D-Man*p*-(1⟶2)-β-D-Glc*p*-OMe (**2**) differing only in the anomeric configuration at the methyl glucoside. Molecular simulations were carried out with five different potential energy functions ranging from pure *in vacuo* to explicit solvent treatment. For comparison, ^{1}H,^{1}H T-ROESY and heteronuclear trans-glycosidic correlation NMR experiments were performed which resulted in proton–proton distances and $^3J_{C,H}$ values, respectively. In addition, interpretation of ^{13}C NMR glycosylation shifts indicated slightly different average conformations of the two disaccharides. From the molecular simulations selected parameters were calculated for comparison to experiments. The combined analysis revealed the conformational region of the disaccharides and showed that the average ψ torsion angle in **2** was more eclipsed than in **1**. Moreover, the translational diffusion coefficients of the disaccharides were determined at 25 °C in D_2O by the Longitudinal Eddy-Delayed experiment which resulted in $D_t = 0.37 \times 10^{-9}$ m^2 s^{-1}. These values were compared to those obtained from molecular dynamics simulations with explicit water as solvent. The relative differences in translational diffusion between the disaccharides and water were similar for experiment and simulation. However, it is well-known that the TIP3P water model overestimates D_t, so also in these simulations.

Introduction

Carbohydrates are ubiquitous in Nature as structural components in plants in the form of cellulose or energy storage in man as glycogen.[1] The outer layers of bacteria contain polysaccharides and glycoconjugates with different functions ranging from structural building blocks to protective shields as well as having pathogenicity enhancement capabilities.[2,3] For an understanding of these large and complex systems the study of disaccharide models with focus on the properties of the glycosidic linkage constitutes a non-trivial but still feasible challenge with respect to the three-dimensional structure including the conformation at the global energy minimum, the flexibility and the dynamics. During the last few years it has become clear that in addition to one or two major conformational states at a glycosidic linkage, "*anti*"-conformers may be populated to a small extent.[4–7] Moreover, it is of interest to be able to monitor also minor conformational changes by simulation and experiment as a function of configurational alterations.

In the present study we have used disaccharides **1** and **2** (Fig. 1) as model compounds. Their conformational properties obtained from molecular simulations in conjunction with experimental NMR data will be evaluated and a comparison between the disaccharides is also carried out.

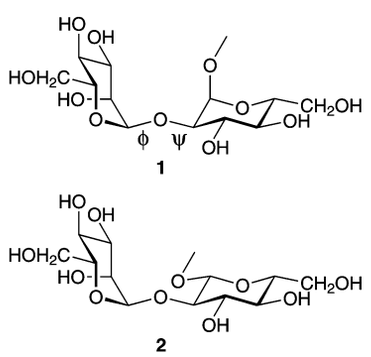

Fig. 1 Schematic of disaccharides **1** and **2** having different anomeric configurations at the *O*-methyl group. Glycosidic torsion angles are denoted by ϕ and ψ.

Materials and methods

General

Synthesis of the disaccharides was described previously together with chemical shift assignments of their ^{1}H and ^{13}C NMR resonances.[8] The atoms of the terminal mannosyl residue are designated with an *m* and those in the glucosyl residue by a *g*. The torsion angles across the glycosidic linkage are defined for ϕ as H1*m*–C1*m*–O3*g*–C3*g* and for ψ as H3*g*–C3*g*–O3*g*–C1*m*.

NMR spectroscopy

The disaccharides were treated with CHELEX 100 in order to remove any paramagnetic ions. The samples were freeze-dried and dissolved in 0.7 cm^3 D_2O to give a total concentration of 100 mM, transferred to 5 mm NMR tubes, and flame-sealed under vacuum after degassing by three freeze–pump–thaw cycles. All NMR experiments were performed on a Varian INOVA 600 spectrometer.

Proton–proton cross-relaxation rates (σ) were measured at 303 K using one-dimensional DPFGSE T-ROESY experiments.[9] Selective excitations were enabled using 25–15 Hz broad i-Snob-2 shaped pulses[10] of 68–113 ms duration. The gradient durations in the initial DPFGSE part were 1 ms and the

 DOI: 10.1039/b111342a

strengths 0.8 and 2.3 G cm^{-1}, respectively. The DPFGSE part was followed by a T-ROESY spin lock with $\gamma B_1/2\pi$ = 2.5 kHz. Spectra were recorded using a width of 1400 Hz and 5600 complex points. For each mixing time 400 transients were used and the total relaxation delay between the transients was 10 s, which corresponds to > 5 T_1. Ten different ^{1}H,^{1}H cross-relaxation delays (mixing times) between 50 and 800 ms were used. Prior to Fourier transformation the FIDs were zero filled and multiplied with a 1 Hz exponential line-broadening factor. Spectra were phased, drift corrected and baseline corrected using a first-order correction, and integrated using the same integration limits at all mixing times.

Integrated auto-peaks were fitted to an exponentially decaying function, and normalized integrals of cross-relaxation peaks were obtained by division of the measured integrals by the extrapolated auto-peak value at zero mixing time. The regression coefficient in the fits was $R > 0.999$ for all auto-peaks. Cross-relaxation build-up curves were obtained from the normalized integrals at different mixing times and the rates were calculated by fitting to a second-order polynomial up to 400 ms. The least-square fits, expressed using the regression coefficient, showed $R > 0.996$ in all cases. When possible, each cross-relaxation rate reported in Table 2 (*vide infra*) is an average of the two obtained from excitations at the different proton resonance frequencies of a proton pair, *e.g.*, in **1** from H1*g* to H2*m* and *vice versa*.

Measurements of the trans-glycosidic carbon–proton coupling constants were performed as a single ^{13}C site selective excitation using a 50 ms half-Gaussian shaped pulse,[11] with a pulsed field gradient version of the pulse sequence.[12] The delay for evolution of the heteronuclear couplings was set to 30 ms and the spectral range was 1400 Hz. The free induction decay (FID) was sampled with 5632 complex data points and the number of transients was 10880. Eight times zero-filling and multiplication of the FID with a 0.3 Hz exponential broadening factor were applied prior to Fourier transformation. Coupling constants were measured directly from the spectra as well as extracted by the *J*-doubling procedure,[13] using 16 delta functions in the frequency domain.

Translational diffusion measurements were performed at 298 K. The deviation from linearity of the pulsed-field-gradient (PFG) pulses over the sample volume was characterized as described by Damberg *et al.*[14] The Stejskal–Tanner spin-echo experiment[15] with an additional gradient pre-pulse, which purges all transverse magnetization from the previous FID and makes the two diffusion encoding gradient pulses more equal was followed by an additional weak gradient during the acquisition period which enables spatial resolution along the *z*-axis. The distribution of the gradient strengths was modeled by a simple truncated linear gradient, resulting in calibrated conditions for a sample with a known translational diffusion coefficient (1% H_2O in D_2O + 1 mg mL^{-1} $GdCl_3$; $D_t = 1.90 \times 10^{-9}$ m^2 s^{-1} at 298 K).[16] The gradient strengths were varied between 0.5 and 14.6 G cm^{-1} in 30 steps. The durations of the PFG pulses were 5 ms and the refocusing delay was 50 ms. Diffusion coefficients of the disaccharides were obtained by the Longitudinal Eddy-Delayed experiment.[17] The gradient strengths were in the range 0.5 to 28.8 G cm^{-1}. The durations of the PFG pulses were 5 ms and the refocusing delay was 100 ms. In addition, dephasing gradients were applied after the second and fourth 90° pulses as well as after the acquisition period. Subsequently, a non-linear two-parameter fit (A_0 and D_t) was performed of the attenuation of signal intensities.

Molecular simulations

Five simulations using Metropolis Monte Carlo (MC) or molecular dynamics (MD) techniques were performed for each disaccharide. In simulation A the molecular mechanics program GEGOP,[18] version 2.7, employed the Hard Sphere *Exo*-Anomeric (HSEA) approach,[19] which uses rigid sugar residues, van der Waals interactions and a torsion potential for ϕ. The simulations *in vacuo* at 300 K employed 10^6 macro steps with a total acceptance ratio of 46 and 44% for **1** and **2**, respectively. The maximum step length for the glycosidic torsion angles was set to 20°.

Simulation B used the Discover program within the InsightII package and the Consistent Valence Force Field (CVFF).[20] The MD simulation *in vacuo* was performed with assignment of initial velocities at 100 K followed by heating during 4 ps to 300 K, where the system was equilibrated for 100 ps. The production run was 5 ns. The simulations employed a relative permittivity of unity, a time step of 1 fs and data were saved every 0.1 ps for analysis.

In simulations C–E the molecular mechanics program CHARMM was used.[21] Simulation C employed the force field CHEAT95,[22] which uses extended atoms for the representation of hydroxy groups, *i.e.*, the hydroxy groups lack the hydrogen and the charge for the hydroxy oxygen is reduced. Assignment of initial velocities at 100 K was followed by heating at 5 K increments during 4 ps to 300 K, where the system was equilibrated for 200 ps. The production run was performed for 3 ns. The simulations employed a distance dependent relative permittivity (*i.e.*, $\varepsilon = r$, where r is the distance between the partially charged atoms), a time step of 1 fs and data were saved every 0.1 ps for analysis.

Simulations D and E used CHARMM (parallel version, C25a2) employing a CHARMM22 type of force field,[23] namely the PARM22 force field (Molecular Simulations Inc., San Diego, CA, USA), which is similar to the carbohydrate force field developed by Ha *et al.*[24] In simulation D the trajectory was based on the Langevin equation, which describes the motions of a particle with a certain mass by a systematic force, a random force and a friction constant.[25] The latter two approximate the influence of solvent on the particle. A value of the collision frequency γ = 50 ps^{-1} was used for heavy atoms.[26] The production run was performed for 30 ns.

In simulation E initial conditions were prepared by placing a disaccharide in a previously equilibrated cubic water box of length 29.97 Å containing 900 TIP3 water[27] molecules, and removing the solvent molecules that were closer than 2.5 Å to any solute atom. This procedure resulted in a system with the disaccharide and 871 and 867 water molecules with **1** and **2**, respectively. Energy minimization was performed with Steepest Descent, 100 steps, followed by Adopted Basis Newton-Raphson until the root-mean-square gradient was less than 0.01 kcal mol^{-1} $Å^{-1}$. Assignment of initial velocities at 100 K was followed by heating at 5 K increments during 8 ps to 300 K, where the system was equilibrated for 200 ps. The production run was performed for 3 ns with the temperature scaled by Berendsen's weak coupling algorithm.[28] Minimum image boundary conditions were used with a heuristic non-bond frequency update and a force shift cutoff[29] acting to 12 Å. The simulations employed a relative permittivity of unity, a time step of 2 fs and data were saved every 0.2 ps for analysis. SHAKE was used to restrain hydrogen-heavy atom bonds,[30] with a tolerance gradient of 10^{-4}.

The geometric criteria for hydrogen bonding were set to an oxygen–hydrogen distance < 2.5 Å and a donor-hydrogen ··· acceptor angle $\Theta > 135°$. Radial distribution functions were integrated for oxygen–oxygen out to 3.5 Å and for hydrogen–oxygen to 2.5 Å to give the corresponding coordination numbers. ^{1}H,^{13}C heteronuclear couplings were calculated using the Karplus relationship devised by Tvaroska *et al.*[31] for each saved conformation, and subsequently averaged. Simulations A–C were performed on an SGI O_2 workstation. Simulations D and E were performed on an IBM SP2 computer at the Center for Parallel Computers, KTH, Stockholm. Simulation E used 16 nodes, resulting in a CPU time of approximately 40 h per ns.

Results and discussion

The initial analysis is based on differences in ^{13}C NMR glycosylation shifts between the two disaccharides and shows that **1** and **2** have different average conformations. Some time ago Bock *et al.*[32] showed that there was a linear dependence on the distance (r) between protons at the glycosidic linkage and the glycosylation shifts ($\Delta\delta_C$) of the carbons involved in the linkage, *i.e.*, C1*m* and C2*g* in the present case, according to:

$$r_{H1m,H2g} = -0.0776\Delta\delta_C + 2.961 \quad (1)$$

It must be kept in mind that the relationship was developed for a *gluco*/*galacto* configuration of the sugar residue at the non-reducing end, *i.e.*, the mannosyl group in this case. The glycosylation shifts were for **1** quite similar with $\Delta\delta_C = 3.6 \pm 0.1$. For **2** they were larger with $\Delta\delta_C = 5.3 \pm 0.3$. The resulting trans-glycosidic H1*m*–H2*g* distance then becomes $r = 2.68$ Å in **1** and $r = 2.55$ Å in **2**. Thus, from ^{13}C glycosylation shifts it can be inferred that $\Delta r_{H1m,H2g} \approx 0.1$ Å between **1** and **2**.

In the same study by Bock *et al.* relationships for the ψ torsional angle dependence on glycosylation shifts were also derived:

$$\psi_{ano} = 5.296\Delta\delta_C - 54.24 \quad (2)$$

$$\psi_{agl} = 5.133\Delta\delta_C - 56.93 \quad (3)$$

where ψ_{ano} and ψ_{agl} refer to the torsion angle ψ derived from glycosylation shifts of the anomeric carbon (C1*m*) and the aglyconic carbon (C2*g*), respectively. Application of the exact glycosylation shifts[8] leads to: $\psi_{ano} = -36°$, $\psi_{agl} = -38°$ in **1** and $\psi_{ano} = -24°$, $\psi_{agl} = -31°$ in **2**. Thus, the difference at this torsion angle should be $\Delta\psi \approx 10°$ between **1** and **2**, with the latter having a more eclipsed conformation. The analysis shows a negative sign for ψ. However, it has been proposed that it is the modulus of ψ, *i.e.*, $|\psi|$, that can be deduced from an analysis based on glycosylation shifts.[33] The subsequent analysis of the disaccharides will try to deduce their conformational preference and subsequently the sign of ψ for the disaccharides.

In the present conformational analysis we have chosen to utilize several force fields to obtain an overview of conformational regions populated to a significant extent. The force fields were implemented in the forms of MC, LD and MD simulations (*vide supra*). Comparison with experimental data will then reveal which simulation(s) agree the best and are consistent with the NMR parameters analyzed.

Results from molecular simulations of **1** and **2** are presented as scatter plots in Fig. 2. Highly populated regions of ϕ/ψ-space are shown as blackened areas as a result of the large number of populated conformational states (each one represented by a dot). The average glycosidic torsion angles are compiled in Table 1. In the broadest sense a similar conformational space is sampled with the five different potentials, for both disaccharides, where a major state is complemented with minor excursions. Detailed analysis reveals a lower magnitude of the ϕ torsion angle in **1** for the A and B force fields with $\phi \approx -40°$, whereas for C–E $\phi \approx -60°$. In general, ϕ in **2** is lower in magnitude (less negative) than in **1**, revealing a systematic difference between the disaccharides. For ψ, **2** shows a more eclipsed average conformation compared to **1** indicating also here a systematic difference. The largest root-mean-square deviations (RMSD) for the glycosidic torsion angles were observed for force field B, *i.e.*, CVFF. In most cases RMSD of $\phi < \psi$ (*cf.* Fig. 2). Of particular interest is the shift of populated states for **1** between the LD simulation (D) and addition of explicit water (E) which leads to a significantly populated state with a positive ψ torsion angle. In **2** the equivalent change in simulation conditions is even more pronounced with $\Delta\phi \approx 25°$ and $\Delta\psi \approx 70°$. Another striking difference between the two disaccharides is the difference for force field D where the changes

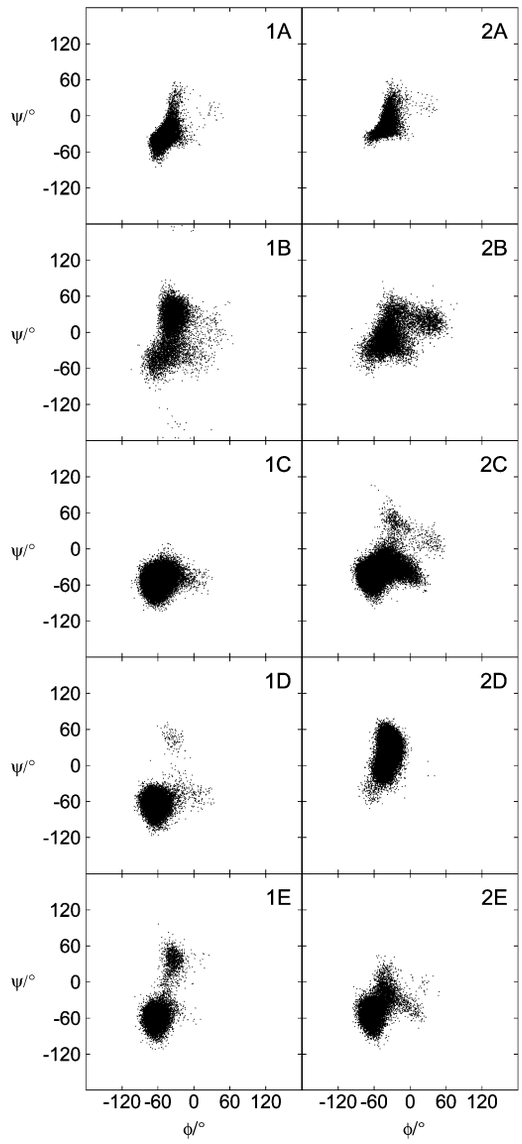

Fig. 2 Scatter plots of ϕ *vs.* ψ from the simulations of **1** (left column) and **2** (right column). The simulations with different potential energy functions are described by A–E (see text for details).

from **1** to **2** are $\Delta\phi \approx 30°$ and $\Delta\psi \approx 80°$ in the positive direction. From the populated regions of conformational space we can obtain different averages for comparison with observed NMR parameters. The conformational properties of the disaccharides can in this way be further analyzed in detail.

NMR parameters used for comparison to simulations were obtained from $^1H,^1H$ cross-relaxation rates, trans-glycosidic heteronuclear coupling constants and translational diffusion coefficients, in addition to the glycosylation shifts discussed above. One-dimensional NMR techniques were used to measure $^1H,^1H$ T-ROESY spectra (Fig. 3). Subsequently, cross-relaxation build-up curves were generated from the experiments with different mixing times (Fig. 4). The cross-relaxation rates, σ, were obtained by fitting to a second order polynomial (Table 2).

When the dynamics of the molecule are unknown and an appropriate reference distance (r_{ref}) can be obtained from, *e.g.*, molecular simulations the unknown distance (r_{ij}) in the molecule can be found by application of the isolated spin-pair approximation (ISPA)[34] according to eqn. (4).

$$r_{ij} = r_{ref}\left(\frac{\sigma_{ref}}{\sigma_{ij}}\right)^{\frac{1}{6}} \quad (4)$$

Table 1 Analysis of simulations A–E for disaccharides **1** and **2** using different potential energy functions. A: HSEA; B: CVFF; C: CHEAT95; D: PARM22/LD; E: PARM22/MD

	1					**2**				
	A	B	C	D	E	A	B	C	D	E
ϕ/°	−47 (12)[a]	−35 (17)	−59 (12)	−64 (11)	−60 (12)	−39 (12)	−29 (27)	−51 (19)	−36 (10)	−60 (12)
ψ/°	−31 (16)	9 (34)	−53 (13)	−65 (13)	−53 (27)	−12 (17)	−4 (23)	−36 (16)	23 (21)	−48 (19)
J_ϕ/Hz	2.7	3.6	1.8	1.4	1.7	3.5	3.6	2.4	3.7	1.8
J_ψ/Hz	3.9	4.0	2.3	1.4	1.9	5.4	4.9	3.6	4.3	2.6
H1*m*–H2*m*/Å[b]	2.56[c]	2.56	2.50	2.51	2.51	2.56[c]	2.56	2.50	2.53	2.50
H1*m*–H2*g*/Å	2.47	2.34	2.91	3.11	2.87	2.33	2.35	2.59	2.20	2.78
H1*m*–H1*g*/Å	2.29	2.94	2.24	2.29	2.27	3.73	3.91	3.20	4.16	2.96
H2*m*–H1*g*/Å	3.94	2.73	4.26	4.47	4.41	4.00	4.46	3.92	4.04	4.17

[a] Root-mean-square deviation in parentheses. [b] Proton–proton distances averaged over trajectories as $\langle r^{-6}\rangle^{-1/6}$. [c] Rigid distance.

Table 2 Cross-relaxation rates σ (s^{-1}) from 1D ^{1}H,^{1}H T-ROESY NMR experiments and the derived proton–proton distances r (Å) for the disaccharides using ISPA

	1		**2**	
Proton pair	σ	r	σ	r
H1*m*–H2*m*	0.071	2.51[a]	0.068	2.50[a]
H1*m*–H2*g*	0.079	2.47	0.091	2.38
H1*m*–H1*g*	0.092	2.40	0.012	3.34
H2*m*–H1*g*	0.005	3.91	0.006	3.75

[a] Reference distance from MD simulation.

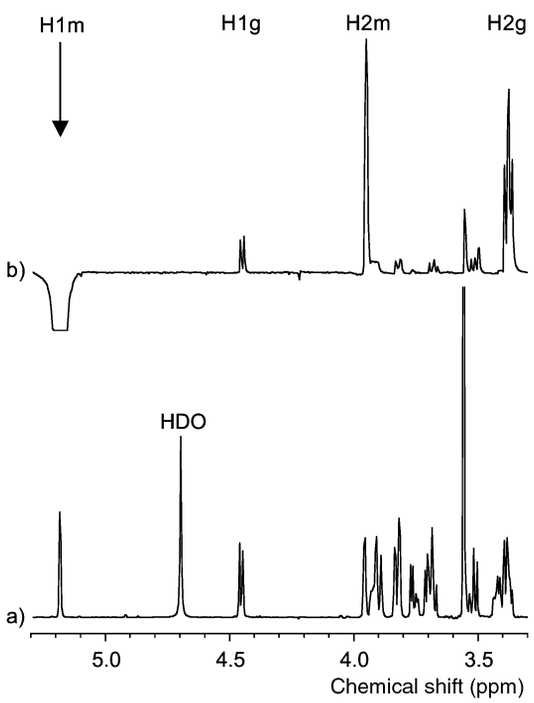

Fig. 3 (a) The ^{1}H NMR spectrum of **2**. (b) 1D ^{1}H,^{1}H T-ROESY spectrum with selective excitation of the resonance from H1*m* and a mixing time of 400 ms. Overhauser effects are observed intra-residually to H2*m* and inter-residually to H1*g* and H2*g*.

The resulting trans-glycosidic proton distances are also given in Table 2. Both disaccharides show a rather short H1*m*–H2*g* distance of ~2.4 Å and a long H2*m*–H1*g* distance of ~3.8 Å. A short distance of ~2.4 Å was observed for H1*m*–H1*g* in **1** and an intermediate distance of ~3.3 Å was present in **2**.

The trans-glycosidic heteronuclear coupling constant for H1*m*–C2*g* in **1** was measured by selective excitation of the C2*g* resonance followed by evolution of the heteronuclear correlation. The anti-phase contribution to the peak shape of

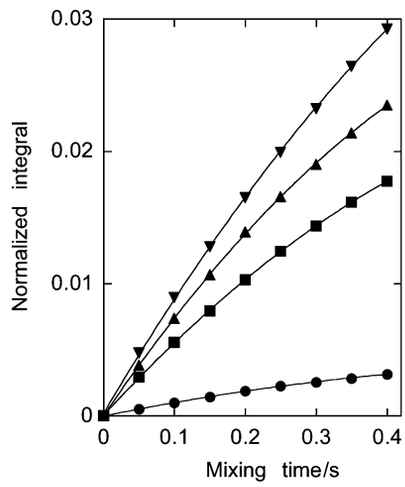

Fig. 4 ^{1}H,^{1}H cross-relaxation build-up curves obtained from the 1D ^{1}H,^{1}H T-ROESY spectra: H1*m*–H2*g* in **2** (▼), H1*m*–H2*g* in **1** (▲), H1*g*–H3*g* in **2** (■) and H1*g*–H1*m* in **2** (●). The first proton of each pair was selectively excited.

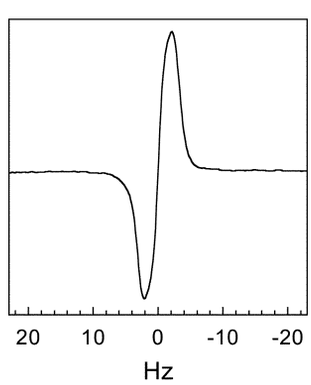

Fig. 5 The resonance from H1*m* in **1** after the long-range experiment with selective excitation of the resonance from C2*g*. The anti-phase separation is equal to the *trans*-glycosidic $^3J_{H,C}$ value which was extracted by the *J*-doubling procedure.

the ^{1}H detected H1*m* resonance (Fig. 5) is equivalent to the $^3J_{C,H}$ coupling constant. This was extracted by the *J*-doubling procedure in which trial coupling constants (*J**) are tested. An integral minimum occurs when $J^* = J_{exp}$ and subsequently a solution is found. The resulting $J_{H1m,C2g}$ = 3.0 Hz in **1**, slightly lower than the 3.4 Hz observed for **2** previously.[35] $J_{H2g,C1m}$ in **1** could not be determined, probably due to ^{1}H spectral overlap under the experimental conditions employed. In **2**, $J_{H2g,C1m}$ = 5.4 Hz.

Comparison of the experimentally determined NMR parameters to those calculated from molecular simulations reveals information on the potential energy functions used to describe

the conformational space populated by the disaccharides. For J_ϕ of **1** the experimentally determined value agrees very well with force field A (HSEA), which is also the least complex one of the five analyzed. For both J_ϕ and J_ψ of **2** the fit between simulation and experiment is excellent with this force field. The agreement with the CHARMM-based force fields C–E is limited and shows a discrepancy too large to be acceptable for a good description of the molecular systems. The proton–proton distances agree in an excellent manner in **1** and quite well in **2**, when force field A is employed. For **2** a fair agreement is also present when force field C (CHEAT95) is used. Similar results were also observed when a glucosyl trisaccharide analyzed by molecular simulations was compared to experimentally derived NMR data, *i.e.*, the best fit was present when the approach based on HSEA was applied.[36] The complexity of the force fields and the difficulty of obtaining excellent agreement with several experimental observables are further emphasized by the addition of explicit water molecules to the CHARMM potentials described by PARM22. Whereas explicit water in the simulation of **1** produces a slightly better fit to experimental data, the reverse is apparent for **2**.

Hydrogen bond analysis of the MD simulations with explicit water revealed inter-residue H-bonds to be of limited significance since they were only present at most a few percent of the simulation time. However, in the absence of explicit solvent inter-residue H-bonds were present, in some simulations to a large extent. These were, *inter alia*, in **1** between HO3*g* and O5*m* present for 74% of the time in simulation B and in **2** between HO3*g* and O5*m* or O6*m* 62% of the time in simulation D. The findings with explicit solvent present were also corroborated by analysis of radial distribution functions and of coordination numbers (data not shown). Thus, the use of explicit water in these MD simulations is important in order to disrupt any artificial intra-molecular H-bonds. Moreover, water may stabilize conformations of the solute carbohydrate molecule, for instance, by acting as a bridge between constituent monosaccharides in a disaccharide.[37]

Translational diffusion measurements of oligosaccharides yield complementary information on average molecular shape.[38] In this study translational diffusion of the disaccharides was investigated both by NMR experiment and the MD simulations. Determination of the translational diffusion coefficient (D_t) for the disaccharides in D_2O utilized the Longitudinal Eddy-Delayed experiment. D_t was obtained by fitting of the signal decay as a function of increasing gradient strength as described by the Stejskal–Tanner equation:

$$A = A_0 \exp[-(\gamma\delta G)^2 (\Delta - \delta/3) D_t] \qquad (5)$$

where A_0 is the signal area without gradients, γ is the magnetogyric ratio of the proton, G is the gradient strength, Δ is the delay between the two gradients and δ is the duration of a gradient pulse. In D_2O at 25 °C we obtained $D_t = 0.36 \times 10^{-9}$ m^2 s^{-1} for **1** and $D_t = 0.37 \times 10^{-9}$ m^2 s^{-1} for **2**. The difference in the value of D_t is within experimental error and we regard $D_t = 0.37 \times 10^{-9}$ m^2 s^{-1} for the two disaccharides as an appropriate description of their translational diffusion under the experimental conditions employed.

From simulation D_t can be obtained by calculating the center-of-mass mean square displacement (MSD) as a function of time where the limiting slope is proportional to $6D_t$.[39] The TIP3P water model used in the MD simulations is well-known to have a larger D_t[40] than experimentally determined ($D_t = 2.3 \times 10^{-9}$ m^2 s^{-1}). A separate simulation of a cubic box, being 40 Å to the side, of TIP3P water molecules resulted in $D_t = 4.8 \times 10^{-9}$ m^2 s^{-1} (data not shown) in good agreement with recent simulations at 300 K, $D_t = 5.4 \times 10^{-9}$ m^2 s^{-1},[41] and at 298 K, $D_t = 5.7 \times 10^{-9}$ m^2 s^{-1}.[42] In the present simulations "bulk water" showed a slightly slower translational diffusion, $D_t = 3.6 \times 10^{-9}$ m^2 s^{-1} (Fig. 6). The disaccharides had $D_t = 1.0 \times 10^{-9}$ m^2 s^{-1} for

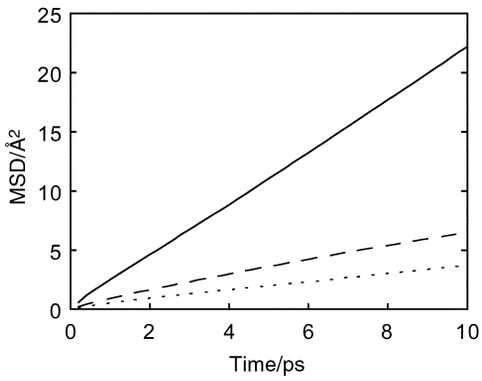

Fig. 6 Mean-square-displacement (MSD) of bulk water (solid line), **2** (dashed line) and **1** (dotted line) from MD simulations.

1 and $D_t = 0.6 \times 10^{-9}$ m^2 s^{-1} for **2**. For comparison to the experimental NMR data we use an average translational diffusion coefficient for the disaccharides from simulation, namely, $D_t = 0.8 \times 10^{-9}$ m^2 s^{-1}. Comparison between experiment and simulation reveals that simulation overestimates D_t by a factor of ~2.[43] However, D_t is slower in D_2O, but only by a factor of 1.2.[44] It is particularly noteworthy that the relative solvent : solute ratio is ~5, both from experiment and simulation. Also, under similar experimental conditions we have previously determined the translational diffusion coefficient of a trisaccharide, $D_t = 0.27 \times 10^{-9}$ m^2 s^{-1},[45] and a pentasaccharide, $D_t = 0.18 \times 10^{-9}$ m^2 s^{-1}.[46] The presently determined D_t for the disaccharides fit well into this series of oligosaccharides.

The five different potential energy functions employed in the molecular simulations and the three different NMR parameters based on (*i*) ^{13}C glycosylation shifts, (*ii*) ^{1}H,^{1}H Overhauser effects, and (*iii*) ^{1}H,^{13}C trans-glycosidic coupling constants reveal conformational differences between the two disaccharides. By application of several force fields the overall conformational region populated by each disaccharide could be identified. The experimental NMR data in this study are of sufficient accuracy to be used both for differentiation of different force fields as well as in bench-marking during development of improved potential energy functions. Notably, the less complex force field in this study, namely HSEA as implemented in the GEGOP program, showed the best agreement with NMR data. Also, the initial indication that the average ψ torsion angle is more eclipsed in **2** than in **1** was fulfilled (Fig. 7). Furthermore, the difference between the

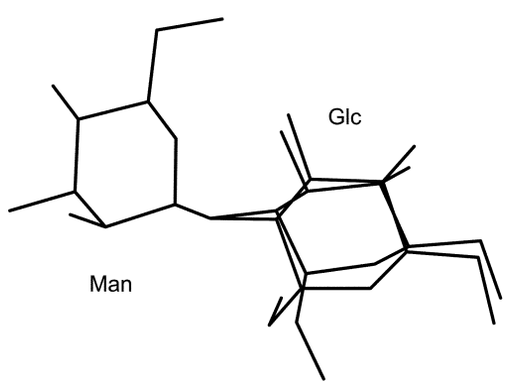

Fig. 7 Overlay based on the mannosyl group of **1** and **2** with glycosidic torsion angles at the average from HSEA simulations.

LD and the MD simulations with explicit water underlines the influence on the effective potential energy function due to solvent. This aspect is important in development of force fields of enhanced quality to utilize the predictive power of molecular simulations.

Acknowledgements

This work was supported by a grant from the Swedish Research Council. We thank the Center for Parallel Computers, KTH, Stockholm, for putting computer facilities at our disposal, R. M. Venable for software for calculation of D_t and Dr J. Jarvet for help with the diffusion measurements.

References

1 J. Lehmann, *Carbohydrates: Structure and Biology*, G. Thieme Verlag, Stuttgart, 1998.
2 *Essentials of Glycobiology*, eds. A. Varki, R. Cummings, J. Esko, H. Freeze, G. Hart and J. Marth, Cold Spring Harbor Laboratory Press, Cold Spring Harbor, NY, 1999.
3 *Endotoxin in Health and Disease*, eds. H. Brade, S. M. Opal, S. N. Vogel and D. C. Morrison, Marcel Dekker, New York, NY, 1999.
4 J. Dabrowski, T. Kosár, H. Grosskurth and N. E. Nifant'ev, *J. Am. Chem. Soc.*, 1995, **117**, 5534.
5 C. Landersjö, R. Stenutz and G. Widmalm, *J. Am. Chem. Soc.*, 1997, **119**, 8695.
6 C. Höög, C. Landersjö and G. Widmalm, *Chem. Eur. J.*, 2001, **7**, 3069.
7 R. Bukowski, L. M. Morris, R. J. Woods and T. Weimar, *Eur. J. Org. Chem.*, 2001, 2697.
8 P.-E. Jansson, L. Kenne, K. Persson and G. Widmalm, *J. Chem. Soc., Perkin Trans. 1*, 1990, 591.
9 A. Kjellberg and G. Widmalm, *Biopolymers*, 1999, **50**, 391.
10 E. Kupce, J. Boyd and I. D. Campbell, *J. Magn. Reson. B*, 1995, **106**, 300.
11 H. Geen and R. Freeman, *J. Magn. Reson.*, 1991, **93**, 93.
12 T. Nishida, G. Widmalm and P. Sándor, *Magn. Reson. Chem.*, 1996, **34**, 377.
13 F. del Río-Portilla, V. Blechta and R. Freeman, *J. Magn. Reson.*, 1994, **111**, 132.
14 P. Damberg, J. Jarvet and A. Gräslund, *J. Magn. Reson.*, 2001, **148**, 343.
15 E. O. Stejskal and J. E. Tanner, *J. Phys. Chem.*, 1965, **42**, 288.
16 R. Mills, *J. Phys. Chem.*, 1973, **77**, 685.
17 S. J. Gibbs and C. S. Johnson, Jr., *J. Magn. Reson.*, 1991, **93**, 395.
18 R. Stuike-Prill and B. Meyer, *Eur. J. Biochem.*, 1990, **194**, 903.
19 H. Thøgersen, R. U. Lemieux, K. Bock and B. Meyer, *Can. J. Chem.*, 1982, **60**, 44.
20 P. Dauber-Osguthorpe, V. A. Roberts, D. J. Osguthorpe, J. Wolff, M. Genest and A. T. Hagler, *Proteins: Struct. Funct. Genet.*, 1988, **4**, 31.
21 B. R. Brooks, R. E. Bruccoleri, B. D. Olafson, D. J. States, S. Swaminathan and M. Karplus, *J. Comput. Chem.*, 1983, **4**, 187.
22 M. L. C. E. Kouwijzer and P. D. J. Groothenhuis, *J. Phys. Chem.*, 1995, **99**, 13426.
23 A. D. MacKerell, Jr., D. Bashford, M. Bellott, R. L. Dunbrack, Jr., J. D. Evanseck, M. J. Field, S. Fischer, J. Gao, H. Guo, S. Ha, D. Joseph-McCarthy, L. Kushnir, K. Kuczera, F. T. K. Lau, C. Mattos, S. Michnick, T. Ngo, T. D. Nguyen, B. Prodhom, W. E. Reiher, III, B. Roux, M. Schlenkrich, J. C. Smith, R. Stote, J. Straub, M. Watanabe, J. Wiórkiewicz-Kuczera, D. Yin and M. Karplus, *J. Phys. Chem. B*, 1998, **102**, 3586.
24 S. N. Ha, A. Giammona, M. Field and J. W. Brady, *Carbohydr. Res.*, 1988, **180**, 207.
25 R. W. Pastor, in *The molecular dynamics of liquid crystals*, ed. G. R. Luckhurst and C. A. Veracini, Kluwer Academic Publishers, Dordrecht, 1994, p. 85.
26 B. J. Hardy, W. Egan and G. Widmalm, *Int. J. Biol. Macromol.*, 1995, **17**, 149.
27 W. L. Jorgensen, J. Chandrasekhar, J. D. Madura, R. W. Impey and M. L. J. Klein, *J. Chem. Phys.*, 1983, **79**, 926–935.
28 H. J. C. Berendsen, J. P. M. Postma, W. F. van Gunsteren, A. DiNola and J. R. Haak, *J. Chem. Phys.*, 1984, **81**, 3684.
29 P. J. Steinbach and B. R. Brooks, *J. Comput. Chem.*, 1994, **15**, 667.
30 J. P. Ryckaert, G. Ciccotti and H. J. C. Berendsen, *J. Comput. Phys.*, 1977, **23**, 327.
31 I. Tvaroska, M. Hricovíni and E. Petráková, *Carbohydr. Res.*, 1988, **189**, 359.
32 K. Bock, A. Brignole and B. W. Sigurskjold, *J. Chem. Soc., Perkin Trans. 2*, 1986, 1711.
33 M. J. Gidley and S. M. Bociek, *J. Am. Chem. Soc.*, 1988, **110**, 3820.
34 J. W. Keepers and T. L. James, *J. Magn. Reson.*, 1984, **57**, 404.
35 C. Höög and G. Widmalm, *Glycoconjugate J.*, 1998, **15**, 183.
36 C. Höög and G. Widmalm, *Arch. Biochem. Biophys.*, 2000, **377**, 163.
37 K. J. Naidoo and J. W. Brady, *J. Am. Chem. Soc.*, 1999, **121**, 2244.
38 C. Monterio and C. Hervé du Penhoat, *J. Phys. Chem. A*, 2001, **105**, 9827.
39 D. Chandler, *Introduction to Modern Statistical Mechanics*, Oxford University Press, Oxford, 1987.
40 S. E. Feller, R. W. Pastor, A. Rojnuckarin, S. Bogusz and B. R. Brooks, *J. Phys. Chem.*, 1996, **100**, 17011.
41 D. van der Spoel, P. J. van Maaren and H. J. C. Berendsen, *J. Chem. Phys.*, 1998, **108**, 10220.
42 P. Mark and L. Nilsson, *J. Phys. Chem. A*, 2001, **105**, 9954.
43 S. Bogusz, R. M. Venable and R. W. Pastor, *J. Phys. Chem. B*, 2001, **105**, 8312.
44 R. Mills and K. R. Harris, *Chem. Soc. Rev.*, 1976, **5**, 215.
45 G. Widmalm and R. M. Venable, *Biopolymers*, 1994, **34**, 1079.
46 T. Rundlöf, R. M. Venable, R. W. Pastor, J. Kowalewski and G. Widmalm, *J. Am. Chem. Soc.*, 1999, **121**, 11847.